Diverging Strains near Threshold: Breakdown of the Elastic Description of a Charge Density Wave Model

Muhittin MUNGAN, Susan N. COPPERSMITH
James Franck Institute, The University of Chicago,
Chicago, IL 60637 - USA
Valerii M. VINOKUR
Material Science Division, Argonne National Laboratories,
Argonne, IL 60439 - USA

Abstract

We analyze the strains near threshold in 1-d charge density wave models at zero temperature and strong pinning. We show that in these models local strains diverge near the depinning threshold and characterize the scaling behavior of the phenomenon. This helps quantify when the underlying elastic description breaks down and plastic effects have to be included.

1. Introduction

The motion of charge density waves (CDWs) [1] belongs to a class of systems, including fluxline lattices in a type II superconductors [2], or magnetically induced Wigner crystals in a 2d electron gas among others [3], in which a deformable periodic structure - the CDW - is driven through a random medium, generated by impurities. The dynamics arises out of a competition between driving force, pinning forces exerted by the impurities on the deformable manifold and the many elastically coupled degrees of freedom of the manifold itself that tend to oppose distortions. Not surprisingly, the behavior of these systems is quite rich.

In the limit of zero temperature and driving force the competition of pinning and elastic forces gives rise to a rather complex energy landscape with metastable configurations corresponding to a pinned interface and energy barriers separating these [4-6]. As a spatially uniform driving force is applied, metastable states are destabilized. With increasing force, the equilibrium configurations of the elastic medium become more and more distorted, relying more strongly on the inhomogeneities of the underlying quenched disorder in order to remain pinned. Thus large local strains build up until a threshold is reached, beyond which there are no metastable states anymore and the elastic structure is depinned. As the elastic force is increased beyond the depinning transition, the motion of the deformable medium is at first plastic, becoming more regular as the uniform

driving force dominates over local pinning forces. Koshelev and Vinokur have proposed a *dynamic melting transition* from a moving liquid phase to a moving solid phase for a $2d$ fluxline lattice [7]. A similar transition has also been predicted for three dimensional CDW systems [8-9].

In this paper we focus on the transition from a pinned to a sliding configuration. Typically, this transition is studied using models in which the deformable structure is described as an elastic medium obeying a linear stress-strain relation. It has been shown by Fisher [10] that in such models the depinning transition can be treated as a dynamic critical phenomenon with the driving force assuming the role of a thermal variable. Furthermore, Coppersmith has given a general argument that shows that strains are expected to diverge near the depinning threshold [11]. Roughly speaking the reason for this is as follows: very close to depinning, weakly pinned segments of the elastic medium have to be held in place by segments experiencing strong local pinning. Since local stresses are transferred along the medium, this means that bulk forces acting on weakly pinned segments have to be balanced by surface forces at the boundaries of strongly pinned segments. If, as the depinning threshold is approached, typical sizes of weakly pinned segments increase, local strains supporting these at their boundaries have to diverge.

The divergence of local strains shows that the elastic description becomes inadequate near threshold. Plastic effects such as tear and reconnection in fluxline lattices and phase slips in the case of CDWs have to be included into the treatment of the depinning transition, possibly altering thereby its nature [12]. Since the elastic description breaks down only sufficiently close to threshold, one does not expect plastic effects to be significant away from the transition. Thus one way of incorporating plasticity is to modify the elastic description only near threshold. In order to do so, the behavior of the strains near threshold within the elastic models has to be determined and this is the purpose of the present paper.

Our goal is to explicitly describe the divergence of local strains near threshold for a $1d$ CDW model, building upon earlier work by Middleton *et al.* [13]. The paper is organized as follows: in section II we describe in detail the model and its relevant features. Section III contains some details concerning numerical implementation. We present our results in section IV and conclude with a discussion, section V.

2. The Model

We study a simplified version of the one-dimensional Fukuyama- Lee-Rice Charge Density Wave (CDW) Hamiltonian [14]. The dynamical variables of this model are the coarse-grained phases ϕ_i that interact with a local impurity potential of strength V and (quenched) impurity phase α_i, uniformly distributed in $(0, 2\pi)$. An external force F acts on the overall system. The Hamiltonian is given by [13-15],

$$H_{CDW} = \frac{1}{2} \sum (\phi_{i+1} - \phi_i)^2 - \sum V \cos(\phi_i + \alpha_i) - F \sum \phi_i. \tag{1}$$

Alternatively, we can think of (1) as the Hamiltonian of a (discretized) elastic string in a potential that is periodic along its transverse and random along its longitudinal direction.

114

In either case the assumption is that the discretization does not affect the dynamics of the large length scales of interest.

The motion of the CDW is purely dissipative. We therefore impose overdamped dynamics,

$$\dot{\phi}_i = -\partial H_{CDW}/\partial \phi_i, \tag{2}$$

and obtain the equations of motion,

$$\dot{\phi}_i = \phi_{i+1} - 2\phi_i + \phi_{i-1} - V \sin(\phi_i + \alpha_i) + F. \tag{3}$$

In the following we briefly review some of the important features of this model. It follows immediately from (3) that if $\phi(t) = \{\phi_i(t)\}$ is a solution, so is $\phi(t) = \{\phi_i(t) + 2\pi k\}$, for any integer k. Thus solutions are uniquely specified upto a rigid translation of all phases by a multiple of 2π.

The dynamics generated by (3) obeys the *no passing rule* [13,16]: If $\phi_i^1(t)$ and $\phi_i^2(t)$ are two solutions such that at $t = 0$,

$$\phi_i^1(0) \le \phi_i^2(0), i = 1, 2, ..., L, \tag{4}$$

then for all $t > 0$

$$\phi_i^1(0) \le \phi_i^2(0), i = 1, 2, ..., L. \tag{5}$$

Depending on the magnitude of F, equations (3) have two types of asymptotic solutions, static ($\dot{\phi}_i = 0$) and sliding ($\dot{\phi}_i \ne 0$). More specifically, for a given realization of the quenched random phases $\{\alpha_i\}$ there is a threshold force $F_T(\{\alpha_i\})$, such that for $F < F_T(\{\alpha_i\})$ all asymptotic solutions are static, *i.e. pinned*, while for $F > F_T(\{\alpha_i\})$ there is a *unique* steady state sliding solution [16]. The possibility of coexisting sliding and and pinned solutions at a given external force F is ruled out by the *no passing rule* [13]. However, the *no passing rule* is a consequence of the elastic description of the deformable medium. In models where plastic effects such as phase slips are included, coexisting static and sliding solutions are possible.

The nature of the metastability in the pinned phase is more readily understood by writing down the *effective Hamiltonian* 'seen' by the ith phase, while keeping the neighboring phases ϕ_{i-1} and ϕ_{i+1} fixed [10.13]:

$$H_i = (\phi_i - \frac{1}{2}(F + \phi_{i+1} + \phi_{i-1}))^2 - V \cos(\phi_i + \alpha_i), \tag{6}$$

such that

$$\dot{\phi}_i = -\frac{\partial H_i}{\partial \phi_i}. \tag{7}$$

Depending on the local *effective field*

$$F_i = F + \phi_{i+1} + \phi_{i-1}, \tag{8}$$

H_i can have multiple local minima. For a static solution each of the phases ϕ_i has to be in one of the local minima of their effective Hamiltonian H_i. A sufficiently large change in

F_i will eventually destabilize a local minimum causing the phase ϕ_i to relax (jump) to the location of the next minimum. In general a change in ϕ_i will affect its neighboring phases and hence will alter the local effective field F_i. Thus the overall response to changes in local phases is far more complex than outlined above, but the qualitative picture is essentially correct.

Drawing on the description given above, Fisher [10] has constructed a mean field theory for the depinning transition in which all phases are coupled to each other. Furthermore, he has argued that the depinning transition in the CDW system (3) can be treated as a dynamic critical phenomenon. In this description the reduced force f,

$$f = \frac{|\, F - F_T \,|}{F_T},\tag{9}$$

plays the role of a thermal variable and a correlation length ξ is defined that provides some measure of the size of a region that responds to a change of local phase ϕ_i. The correlation length diverges near threshold and hence finite size scaling is required to extract information from the finite systems that we simulate. We will get back to this when we present our results.

3. Numerical Implementation

Equations (3) with periodic boundary conditions, $\phi_i = \phi_{i+L}$, were numerically integrated using a fourth order Runge Kutta method with adaptive stepsize as described in [17]. The characteristic strength V of the impurity potential was taken to be 2.5.

In order to treat finite size effects and to sample the quenched randomness, we carried out simulations of different sizes L and realizations of the impurity phases $\{\alpha_i\}$. Specifically, for the behavior below threshold, we studied 4096, 2048, 1024, 512, 256, 128, and 64 random realizations for system sizes $L = 16, 32, 64, 128, 256, 512,$ and 1024, respectively. The dynamics above threshold suffered from large relaxation times and we will present only preliminary data for sizes $L = 128$, and 256 with 16 and 8 realizations each.

For each realization of the random impurity phases, the threshold force F_T was obtained first. This was done using a bisection method [13]. One first determines a lower and upper bound for the threshold force, such that there is a static solution for the lower bound, but none for the upper bound. Next this interval is bisected, yielding a better bound for the threshold force. This procedure is continued until the threshold force is bracketed within an interval of satisfactory accuracy. In our simulations we use an accuracy of 10^{-4}. Once the threshold force of a realization is determined (to satisfactory accuracy), static configurations were computed at reduced forces

$$f_i = \frac{F_T - F_i}{F_T} = 2^{-i/2}, i = 0, 1, 2, ..., 27\tag{10}$$

as well as the threshold force.

The search for a static configuration was carried out in two stages: (i) the system is evolved from an initial configuration via numerical integration of the equations of motion

until the LHSs of (3), *i.e.* the time derivatives, are all within an interval (initially $\pm 10^{-3}$) of zero, or all phases have moved by at least 2π. In the latter case the simulation was terminated, with no static solution found, since solutions are periodic with respect to rigid translations of multiples of 2π, and the *no-passing rule* assures that a static solution could not have been missed, as explained in the previous section. In the former case, when all time derivatives are sufficiently small, the configuration just found is used as an initial guess for a Newton Raphson scheme (ii) to find the solution, for which the gradients are zero. If the Newton Raphson scheme iterated the initial configuration away by at least 2π, the iteration was terminated and stage (i) continued with a reduction of the tolerance interval by a factor of 10 (this was done to prevent immediate or excessive reentrance into the second stage). Experience showed that the switch between the first and second stage never occurred more than two times, so that a reduction of the tolerance interval to the accuracy of the simulation was not a serious concern. Typically static solutions found by the Newton Raphson scheme were observed to have a maximum residual LHS of $10^{-9} - 10^{-11}$, much lower than the time derivatives upon entrance into stage (ii).

The (unique) steady state solutions above threshold were determined for sizes $L = 128$, and 256 with 15 reduced forces per size per realization, given by

$$f_i = \frac{F_i - F_T}{F_T} = 2^{3-i}, i = 0, 1, ..., 14. \tag{11}$$

In order to facilitate comparison, the random realization of phases were drawn from the set of those used for the simulations below threshold.

The determination of the steady state solution was carried out using the periodicity in its phases. Given an initial configuration, a particular phase, $\phi_1(\bar{t}_n)$ is picked and the system evolved until a time $\bar{t}_{n+1}$ when

$$\phi_1(\bar{t}_{n+1}) = \phi_1(\bar{t}_n) + 2\pi. \tag{12}$$

The current configuration was compared with the previous one to check for periodicity and the procedure repeated until the max norm between the two configurations defined as

$$\|\phi(\bar{t}_{n+1}) - \phi(\bar{t}_n)\| \equiv \max_i \{\phi(\bar{t}_{n+1}) - \phi(\bar{t}_n)\} - 2\pi, \tag{13}$$

was smaller than a set tolerance, taken to be 10^{-3}.

It should be emphasized that the numerical strategy is relatively efficient, because of the *no-passing rule*. As described in the previous section, when plastic effects, such as phase slips, are incorporated into the equations of motion, the *no-passing rule* does not hold anymore and the numerical computations become more intensive. This is another reason for our general approach to describe the breakdown of the elastic description near the depinning transition in order to find out how this will be modified in the presence of plasticity.

4. Results

Figure 1 shows the various static configurations ϕ_j of a sample of size $L = 100$. As the

external force F is increased from zero ($f = 1$) to the sample threshold force F_T ($f = 0$), local segments of larger size jump into new equilibirium states and strains s_j defined by
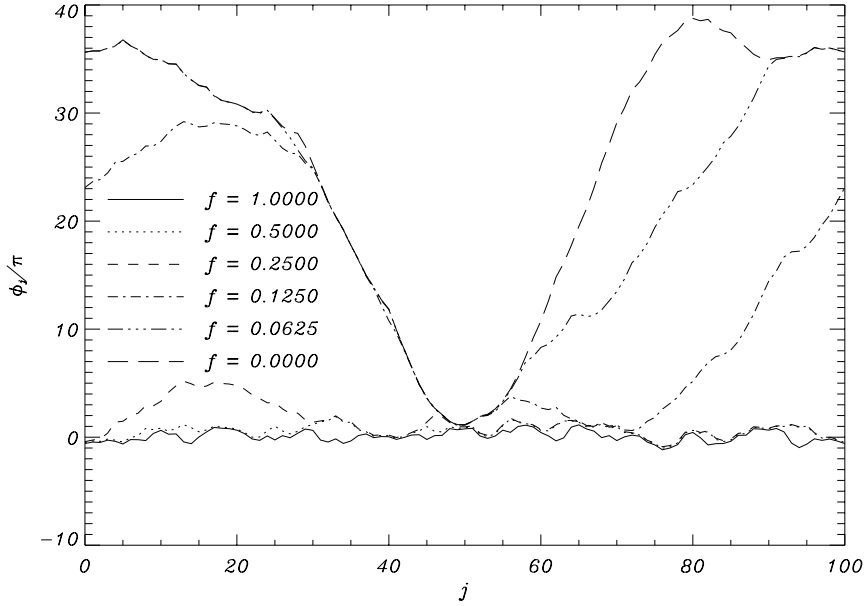

Figure 1. Equilibrium configurations of a $L = 100$ CDW system. Reduced forces f are as indicated, with $F_T = 1.3734$ and $V = 2.5$.

$$s_j = \mid \phi_{j+1} - \phi_j \mid, \tag{14}$$

build up.

We next plot in Figure 2 the distribution of local strains for $L = 512$ at various reduced forces, obtained from our numerical simulations.

The distributions become broader as the threshold force is approached, indicating increasing strains. To illustrate this further, we plot in Figure 3 the average strain obtained from the distributions as a function of reduced force for different system sizes.
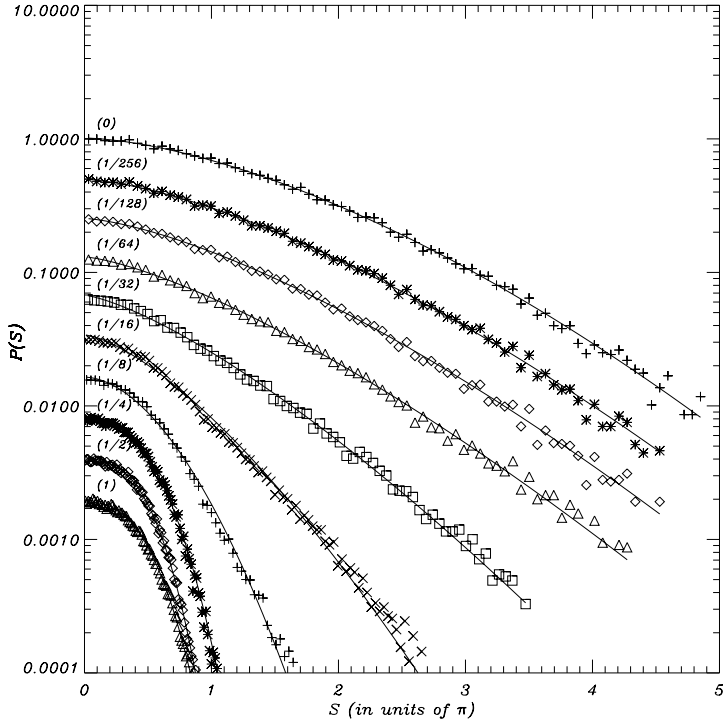
118

Figure 2. Strain Distributions obtained from the data of 128 realizations of a $L = 512$ CDW system. Reduced forces are indicated in parentheses. Solid lines are best fits to a stretched exponential, $P(s) \sim \exp(-cs^{\alpha})$. Curves have been offset vertically for clarity.

Figure 3 shows that the average strains are independent of system size L for small forces $f \to 1$ and increase as F_T is approached ($f \to 0$). As $f \to 0$ the average strains saturate to values that increase with system size. Moreover, the point of saturation moves closer to the threshold as the system size L is increased.

These qualitative features are readily explained by treating the depinning transition as a dynamic critical phenomenon, as argued by Fisher [10]. In this description the saturation near threshold is a finite size effect that is due to the correlation length being of order of the system size. The following is a brief review of the theory of finite size scaling, further details can be found for example in [18] and references therein.

Suppose that for an infinite size system, the correlation length ξ scales like

$$\xi \sim f^{-\nu_s}, \tag{15}$$

and a quantity s scales like

$$s \sim f^{-\gamma} \tag{16}$$

119

near the transition. In the theory of finite size scaling effects due to the finite size of the system modify the scaling law (16) to be of the form

$$s = L^{\gamma/\nu}\bar{\Psi}(L/\xi) = L^{\gamma/\nu}\Psi(fL^{1/\nu}), \tag{17}$$

subject to the following asymptotic conditions on Ψ: (i) when $L \gg \xi$, the scaling law 16 is recovered, $\Psi(x) \sim x^{-\gamma/\nu}$ for large x, while (ii) for $L \ll \xi$, s should be independent of f yielding $\psi(x) \to const.$ as $x \to 0$.

If the scaling form (17) is correct then plots of $sL^{-\gamma/\nu}$ vs $fL^{1/\nu}$ for various sizes L should produce curves that collapse on each other.

A scaling plot of the average strains S_{av} for sizes $L \geq 128$ is shown in Figure 4. The collapse gets less satisfactory when smaller system sizes are included. The best values for the scaling exponents are obtained as $\nu = 1.6 \pm 0.1$ and $\gamma/\nu = 0.45 \pm 0.01$, yielding $\gamma = 0.72 \pm 0.05$. The uncertainties in the numbers given are an estimate only and reflect the range of scaling exponents over which the data collapse does not change significantly.
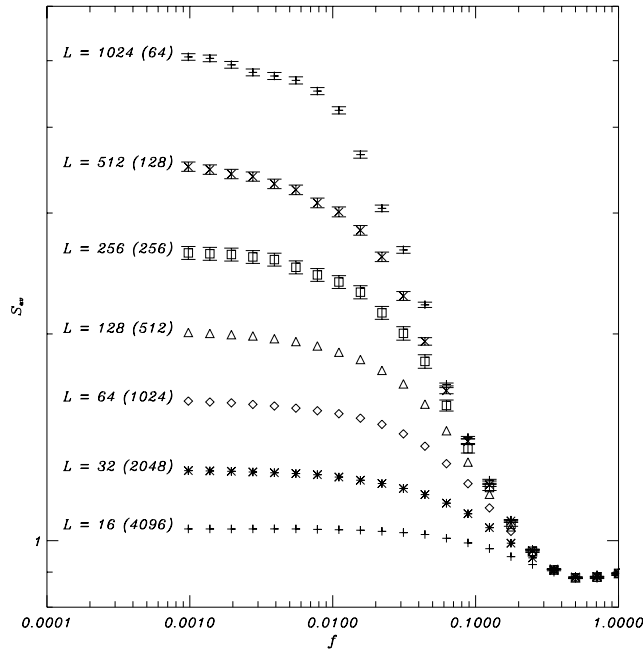

Figure 3. Plot of average strain S_{av} in units of π against reduced force f for various system sizes L. Indicated in parentheses are the number of realizations averaged over. Errorbars indicate the error in the mean, obtained from averaging the mean strains of each realization (shown only for sizes $L = 256$, $L = 512$, $L = 1024$, for clarity). Errors increase as the threshold is approached and are less than 5%.

A similar analysis can be carried out for the standard deviation of the strain distributions. The results are not shown here, but it turns out that the scaling exponents are equal within their respective accuracies to those obtained for the average strains. It is possible to fit the strain distributions to a stretched exponential functional form $P(s) \sim \exp(-cs^\alpha)$. Shown also in Figure 2 are the best fits of the $L = 512$ strain distributions to this functional form (solid lines).
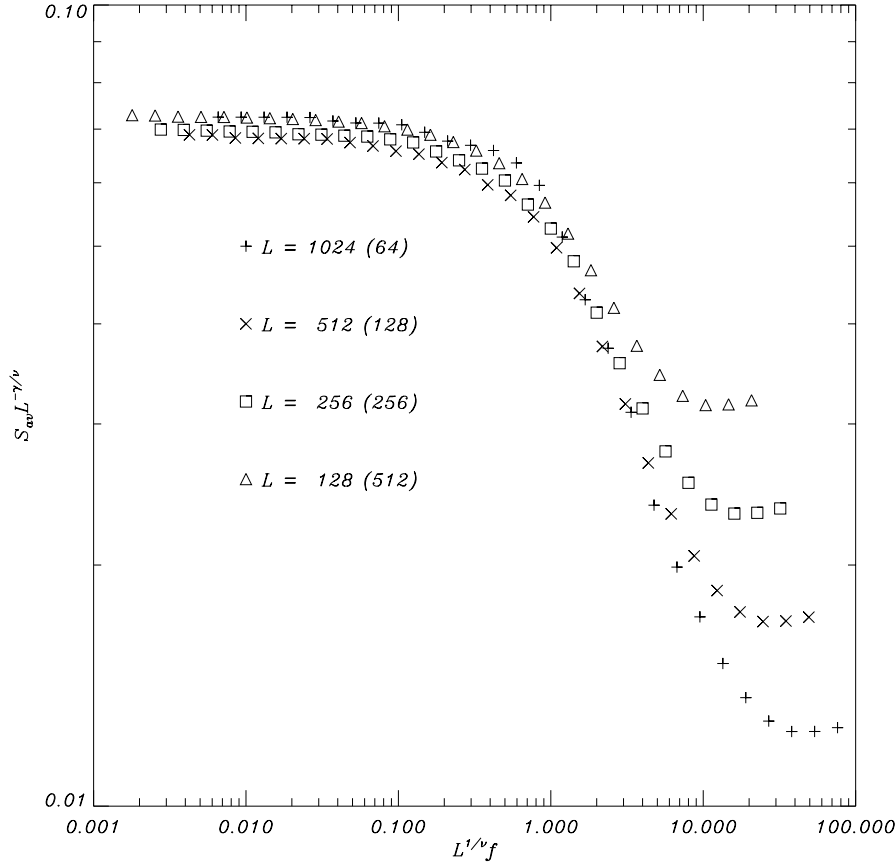

Figure 4. Finite size scaling function for the average strain S_{av} (in units of π). The best collapse is achieved for $\nu = 1.6 \pm 0.1$ and $\gamma/\nu = 0.45 \pm 0.01$. Indicated in parentheses are the number of realization from which the averages were obtained.

Figure 5 shows some preliminary data for the steady-state strains above threshold. The simulations suffer from large relaxation times for large system sizes. We have not acquired enough data yet to make quantitative predictions. However, figure 5 shows

that the average strain decreases with increasing driving force, in agreement with the expectation that in this regime pinning forces become less important. Comparing Figure 5 with the corresponding Figure 3 for average strains below threshold, it seems that the finite- size saturation of the average strain is reached at higher reduced forces.

If this result is borne out by more extensive simulations, this implies that the correlation length diverges faster above threshold, which could be due to a larger prefactor in (15), or different scaling exponents ν on both sides of the depinning transition. Especially the latter possibility is rather intriguing, however more work needs to be done to characterize this.
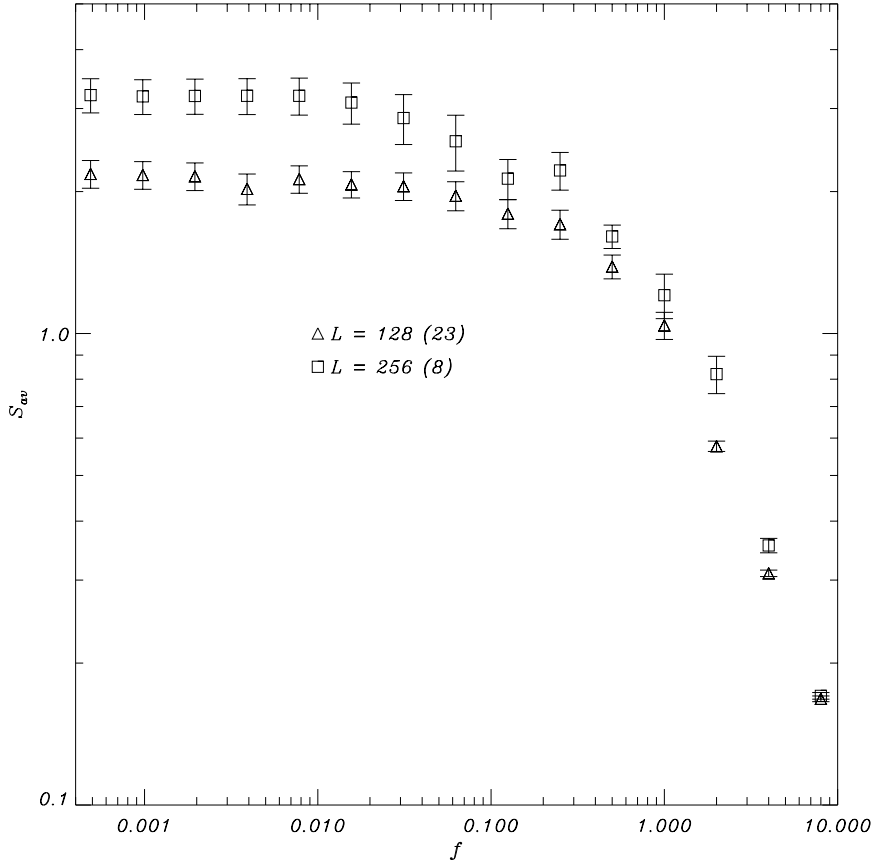

Figure 5. Preliminary data for the average Strains S_{av} above threshold. Results were obtained from averaging strains over 23 and 8 realizations of size $L = 256$ (boxes) and $L = 128$ (triangles). Errorbars indicate the error in the mean obtained from averaging the main strains of each realization.

Middleton has studied in his thesis [13] the dependence of the average steady-state CDW velocity v defined by

$$v = \lim_{T \to \infty} \frac{1}{LT} \sum_j (\phi_j(T) - \phi_j(0)), \qquad (18)$$

on the reduced force f. He finds that the f-v relation in one dimension exhibits very weak size dependence, if at all. We observed similar results in our simulations and also found that it takes a relatively short time compared to the period of the steady-state solution for v to approach its asymptotic value. We find however, that the relaxation of the strains to their steady-state values takes place on much larger times scales (upto a factor of thousand for large system sizes). The reason for the difference of time scales is most readily seen by considering the case of large external driving force F. In this limit the impurity forces can be neglected and equations (3) are solved by a discrete Fourier transform of ϕ_j. The average velocity is determined by the zero-mode and does not evolve at all, while all other modes decay exponentially with a characteristic time given in the limit of large L/k by $\tau_k \approx (L/2\pi k)^2$. Thus to this order, the relaxation time for the configurations increases with the square of the system size, while the average velocity remains constant.

5. Discussion

Using finite-size scaling we have demonstrated the divergence of strains near the depinning transition. Our results have been obtained for the case where the transition is approached from the pinned state. The uniqueness of the solution in the sliding state as well as the pinning state very close to threshold, strongly suggest a similar divergence when the transition is approached from the sliding state. Our preliminary data for the average strains above threshold supports this.

Earlier findings show that the relation between average steady-state velocity and driving force does not exhibit any appreciable size dependence [13]. Our preliminary data clearly shows that the average strains are size dependent. We believe that this dependence on system size is due to the very different relaxation mechanisms for the average velocity and configurations, as seen in the strong forcing limit.

A more detailed investigation of the dynamics above threshold and the inclusion of temperature will be taken up in a future publication.

Acknowledgments

References

[1] G. Grüner, *Rev. Mod. Phys.* **60**, 1129 (1988).

[2] G. Blatter, M. V. Feigelman, V. B. Geshkenbein, A. I. Larkin, and V. M. Vinokur, *Rev. Mod. Phys.* **66**, 1125 (1994).

[3] E. Y. Andrei, G. Deville, D. C. Glattli, F. I. B. Williams, E. Paris and B. Etienne, *Phys. Rev. Lett.* **60**, 2765 (1988); R. L. Willet, in *Phase Transitions and Relaxations in System with Competing Energy Scales*, T. Riste and D. Sherrington, eds., Nato ASI series vol. 415, p. 367 (Kluwer Academic Pub., Dordrecht, 1993); and references therein.

[4] M. Kardar, *Lectures on directed Paths in Random Media*, Proceedings of the Les Houches Summer School on Fluctuating Geometries in Statistical Mechanics and Field Theory, also: *preprint* cond-mat/9411022.

[5] L. V. Mikheev, B. Drossel and M. Kardar, *Phys. Rev. Lett.* **75**, 1170 (1995).

[6] V. M. Vinokur, M. C. Marchetti and L. Cheng, *Phys. Rev. Lett.* **77**, 1845 (1996).

[7] A. E. Koshelev and V. M. Vinokur, *Phys. Rev. Lett.* **73**, 3580 (1994).

[8] L. Balents and M. P. A. Fisher, *Phys. Rev. Lett.* **75**, 4270 (1995).

[9] V. M. Vinokur and T. Nattermann, *preprint* cond-mat/9708175.

[10] D. S. Fisher, Phys. Rev. Lett. **50**, 1496 (1983), *Phys. Rev. B* **31**, 1396 (1985).

[11] S. N. Coppersmith, *Phys. Rev. Lett.* **65**, 1044 (1990); *Phys. Rev. B* **44**, 2887 (1991).

[12] S. N. Coppersmith and A. J. Millis, *Phys. Rev. B* **44**, 7799 (1991) *and references therein.*

[13] A. A. Middleton, PhD Thesis, Princeton University (1990); A. A. Middleton and D. S. Fisher, *Phys. Rev. B* **47**, 3530 (1993).

[14] H. Fukuyama, P. A. Lee, *Phys. Rev. B* **17**, 535 (1977); P. A. Lee, T. M. Rice, *Phys. Rev. B* **19**, 3970 (1979); K. B. Efetov, A. I. Larkin, *Zh.Eksp.Teor.Fiz.* **72**, 2350 (1977) [*Sov. Phys. JETP* **45**, 1236 (1977)].

[15] L. Sneddon, M. C. Cross, D. S. Fisher, *Phys. Rev. Lett.* **49**, 292, (1990); L. Pietronero, S. Strässler, *Phys. Rev. B* **28**, 5863 (1983); H. Matsukawa, H. Takayama, *Solid State Commun.* **50**, 283 (1984).

[16] A. A. Middleton, *Phys. Rev. Lett.* **68**, 670 (1992).

[17] W. H. Press, B. P. Flannery, S. A. Teukolsky, W. T. Vetterling, *Numerical Recipes, The Art of Scientific Computing*, Cambridge University Press, Cambridge (1989).

[18] J. L. Cardy (editor), *Finite-Size Scaling*, North Holland, Amsterdam (1988).